

Universal equation of state for wave turbulence in a quantum gas

Lena H. Dogra¹, Gevorg Martirosyan¹, Timon A. Hilker^{1,2}, Jake A. P. Glidden¹, Jiří Etrych¹, Alec Cao¹, Christoph Eigen¹, Robert P. Smith³, and Zoran Hadzibabic¹

¹ *Cavendish Laboratory, University of Cambridge, J. J. Thomson Avenue, Cambridge CB3 0HE, United Kingdom*

² *Max-Planck-Institut für Quantenoptik, 85748 Garching, Germany*

³ *Clarendon Laboratory, University of Oxford, Parks Road, Oxford OX1 3PU, United Kingdom*

(Dated: May 8, 2023)

Boyle’s 1662 observation that the volume of a gas is, at constant temperature, inversely proportional to pressure, offered a prototypical example of how an equation of state (EoS) can succinctly capture key properties of a many-particle system. Such relations are now cornerstones of equilibrium thermodynamics [1]. Extending thermodynamic concepts to far-from-equilibrium systems is of great interest in various contexts including glasses [2, 3], active matter [4–7], and turbulence [8–11], but is in general an open problem. Here, using a homogeneous ultracold atomic Bose gas [12], we experimentally construct an EoS for a turbulent cascade of matter waves [13, 14]. Under continuous forcing at a large length scale and dissipation at a small one, the gas exhibits a non-thermal, but stationary state, which is characterised by a power-law momentum distribution [15] sustained by a scale-invariant momentum-space energy flux [16]. We establish the amplitude of the momentum distribution and the underlying energy flux as equilibrium-like state variables, related by an EoS that does not depend on the details of the energy injection or dissipation, or the history of the system. Moreover, we show that the equations of state for a wide range of interaction strengths and gas densities can be empirically scaled onto each other. This results in a universal dimensionless EoS that sets benchmarks for the theory and should also be relevant for other turbulent systems.

The framework of thermodynamics provides an effective way to characterise equilibrium states of macroscopic systems without need for a detailed microscopic description. It can also be applied to near-equilibrium situations, such as linear transport, where the equilibrium state variables such as temperature are locally (in space and time) well defined. A major ongoing challenge is to develop an equally effective framework for far-from-equilibrium systems. Such systems do not have all equilibrium variables defined even locally, but can nevertheless have well-defined stationary (albeit non-thermal) states, which in principle are amenable to thermodynamics-like treatments, including being describable by an equation of state (EoS) (Fig. 1a). Specifically, if quantities that describe fundamentally non-equilibrium phenomena, such as the energy dissipation rate, have values that are constant in time, they can take on the role of non-equilibrium state variables.

A turbulent cascade with matching energy injection (at one length scale) and dissipation (at a different one) is a paradigmatic stationary non-thermal state, sustained by a constant momentum-space energy flux that flows from the injection to

the dissipation scale [17]. From ocean waves [18] to interplanetary plasmas [19] and financial markets [20], such cascades generically result in power-law spectra of the various relevant quantities, with problem-dependent exponents.

For a given exponent, a cascade spectrum is fully defined by its amplitude. Famously, for hydrodynamic vortex turbulence in an incompressible fluid, dimensional analysis relates this amplitude to the magnitude of the underlying scale-invariant flux [21–23]; this amplitude-flux relation then serves as an equilibrium-like EoS. In general, dimensional analysis is insufficient, but for wave turbulence there are solvable approximate models that give more physical insight and also imply EoS-like amplitude-flux relations [11, 13, 14].

We study wave cascades from small to large wavenumbers k (large to small length scales) using a Bose gas held in a cylindrical optical-box trap [24, 25] and driven on a system-

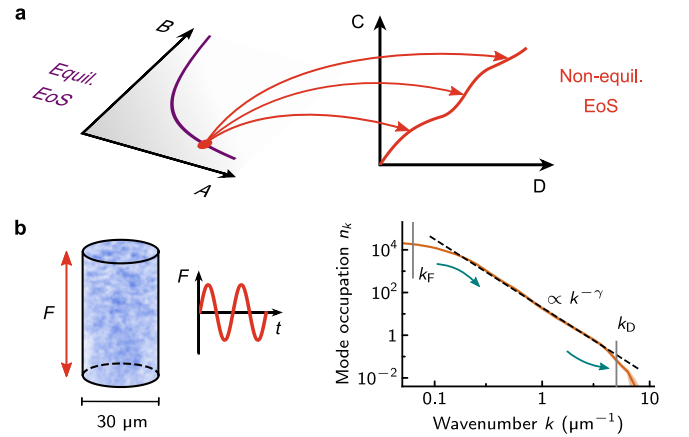


FIG. 1. Far-from-equilibrium equation of state and our experiment. **a**, An EoS describes possible states of a macroscopic system by giving the relation between the state variables such as pressure or chemical potential. Here, A and B are some generic equilibrium state variables, all equilibrium states lie in the A – B plane, and out of each of them one can create (arrows) countless far-from-equilibrium ones. If the latter are stationary, they might still obey an EoS with new state variables C and D . **b**, Using an atomic Bose gas, we study a paradigmatic far-from-equilibrium stationary state, a turbulent cascade with matching energy injection at one length scale (k_F^{-1}) and dissipation at another (k_D^{-1}). Left: our gas is held in a cylindrical optical box (cartoon) and continuously driven on a large length scale by a time-periodic force F . Right: in steady state, the gas exhibits a highly non-thermal, but stationary, power-law momentum distribution $n_k \propto k^{-\gamma}$, with $\gamma = 3.2$ (Methods).

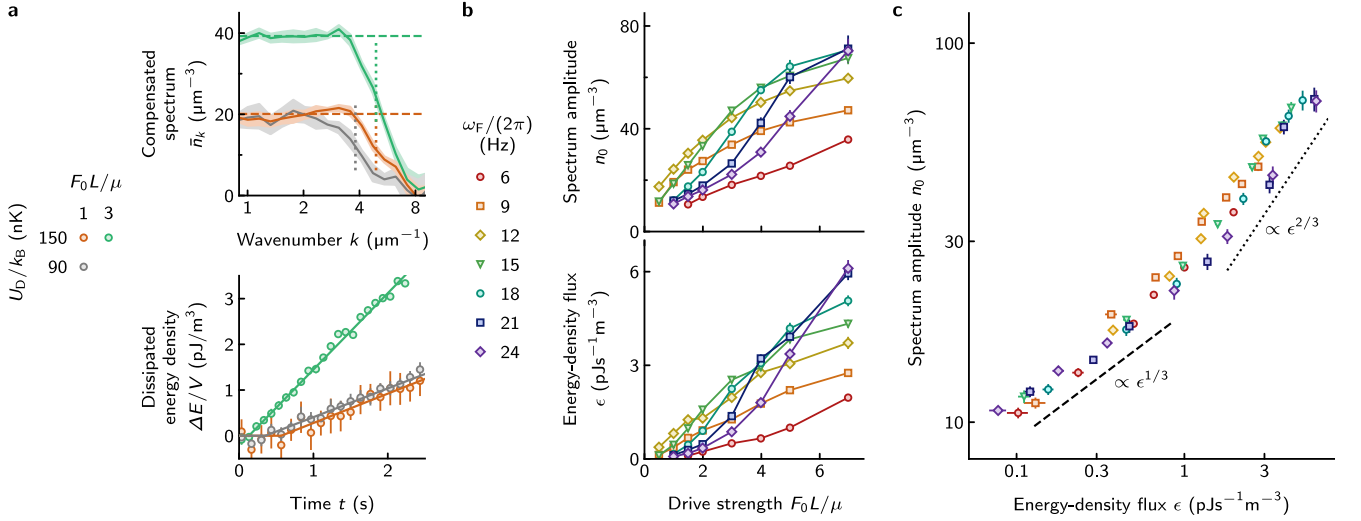


FIG. 2. Constructing an equation of state for a turbulent quantum gas. Here we explore turbulent steady states in a gas with initial density $n = 5.7 \mu\text{m}^{-3}$ and interaction strength $a = 100 a_0$; the chemical potential, $\mu \propto na$, is $k_B \times 4.7 \text{ nK}$, and the healing length is $\xi = 1.2 \mu\text{m}$. The gas is driven by a spatially uniform force $F_0 \sin(\omega_F t)$, with variable F_0 and ω_F . The trap depth U_D , which sets the dissipation scale $k_D \propto \sqrt{U_D}$, is $k_B \times 150 \text{ nK}$, except for the grey data in **a**, where it is $k_B \times 90 \text{ nK}$. **a**, Examples of the steady-state momentum distributions n_k and the corresponding energy fluxes ϵ , for $\omega_F / (2\pi) = 15 \text{ Hz}$. Top: we plot the compensated spectra $\tilde{n}_k = k^3 (k\xi)^{0.2} n_k$ (see text), so the spectrum amplitudes n_0 are seen in the plateaus indicated by the horizontal dashed lines; the vertical dotted lines indicate the k_D values. Bottom: we plot the dissipated energy per unit volume, $\Delta E / V = U_D \Delta N / V$, where ΔN is the total number of atoms that have left the trap at k_D , and V is the box volume, so ϵ (dissipation rates) are the slopes of the data; the solid lines show piece-wise linear fits. Both n_0 and ϵ increase with F_0 , but are independent of k_D . **b**, n_0 and ϵ as a function of F_0 for different ω_F . The curves for different ω_F have different shapes and cross due to nonlinear effects of strong driving on the excitation resonance. **c**, Eliminating the drive parameters F_0 and ω_F , and directly relating n_0 to ϵ , collapses all the data onto a single EoS-like curve. The dashed and dotted lines are guides to the eye. The shading and error bars in **a** reflect standard errors of measurement, while the error bars in **b** and **c** reflect standard fitting errors.

size length scale by a spatially uniform time-periodic force F (Fig. 1b, left) [15]. In steady state, the cascade is characterised by an isotropic momentum distribution (Fig. 1b, right): $n_k(\mathbf{k}) \propto k^{-\gamma}$, with $\gamma = 3.2(2)$ in agreement with the theory of weak wave turbulence (WWT) [13, 14, 26, 27]; here n_k is the mode occupation, \mathbf{k} is the wavevector and $k = |\mathbf{k}|$. In theory, $n_k = n_0 k^{-3} f(k)$, where n_0 is the cascade amplitude and f is a slowly varying dimensionless function, such that asymptotically $n_k \sim k^{-3}$ for $k \rightarrow \infty$, while in a finite (experimentally relevant) k -range n_k is close to a power-law with an effective γ slightly larger than 3 (Methods). To experimentally extract n_0 from a finite k -range, we model f by $(k\xi)^{-0.2}$, where $\xi \approx 1 \mu\text{m}$ is the healing length (Methods). The cascade terminates by atoms leaving the trap at k_D (the dissipation scale) set by the trap depth, and the rate at which they leave gives the steady-state energy-density flux ϵ [16]. We explore the relationship between n_0 and ϵ for different F , k_D , box sizes, and microscopic gas parameters.

We start with an equilibrium Bose–Einstein condensate of 2×10^5 atoms of ^{39}K in the lowest hyperfine ground state, held in a trap of length $L = 50 \mu\text{m}$ and radius $R = 15 \mu\text{m}$, so the gas density is $n = 5.7 \mu\text{m}^{-3}$. Using the Feshbach resonance at 402.7 G [28] we set the s -wave scattering length a to $100 a_0$, where a_0 is the Bohr radius, so the chemical potential is $\mu = 4\pi\hbar^2 na / m = k_B \times 4.7 \text{ nK}$ and $\xi = \hbar / \sqrt{2m\mu} = 1.2 \mu\text{m}$; here \hbar is the reduced Planck constant,

k_B the Boltzmann constant, and m the ^{39}K atom mass. The force $F = F_0 \sin(\omega_F t)$, created by a magnetic field gradient, primarily injects energy into the lowest phonon mode [15, 29], at $k_F = \pi / L = 0.06 \mu\text{m}^{-1} \ll 1 / \xi$, so the natural scales for the drive strength F_0 and frequency ω_F are set, respectively, by μ / L and $\sqrt{\mu / m} k_F \approx 2\pi \times 10 \text{ Hz}$. The trap depth is $U_D = k_B \times 150 \text{ nK} \gg \mu$, so $k_D = \sqrt{2mU_D} / \hbar = 4.9 \mu\text{m}^{-1}$.

In Fig. 2a we show measurements of the steady-state n_k and ϵ for two drive strengths and fixed ω_F . In the top panel we plot compensated spectra, $\tilde{n}_k = k^3 (k\xi)^{0.2} n_k$, so the n_0 values are seen in the plateaus indicated by the dashed lines. In the bottom panel, the corresponding ϵ values are given by the slopes of the data, which are essentially constant over several seconds; initially the slope is zero (there is no dissipation) until the flux reaches k_D and the steady state is established [16, 29], while at long times (not shown) the condensate gets depleted. We also show, for $F_0 = \mu / L$, that neither n_0 nor ϵ change if we change k_D by reducing U_D / k_B to 90 nK .

In Fig. 2b we present a systematic study of the cascade amplitudes and fluxes for different drive parameters F_0 and ω_F . Both n_0 and ϵ monotonically increase with F_0 for any fixed ω_F , but individually they depend in a complicated way on both F_0 and ω_F , with the different- ω_F curves having different shapes and even crossing due to nonlinear effects of strong driving on the excitation resonance [15, 30].

However, as we show in Fig. 2c, plotting n_0 versus ϵ re-

veals a unique EoS-like relation. All the data from Fig. 2b collapse onto a single curve, showing that the steady-state n_k depends only on the underlying flux and not on the details of its injection. Also note that n_0 is, for fixed k_D , proportional to the energy density, and hence pressure, so although we extracted it from the full microscopic n_k , it could in principle be a macroscopic observable.

In Fig. 2c, the low- ϵ data are consistent with the scaling $n_0 \propto \epsilon^{1/3}$ from perturbative WWT theory [13, 14]; modelling a turbulent Bose gas by the classical-field Gross-Pitaevskii equation (GPE) [13–15, 27, 31] and assuming that the cascade transport is driven by four-wave mixing of incoherent waves, without any role played by the coherent condensate, gives an analytical prediction $\epsilon \propto \hbar^3 n_0^3 a^2 / m^2$. However, for large ϵ we observe significant departure from this scaling, suggesting qualitatively different behaviour. Recently there has been a lot of interest in different regimes of turbulence in strongly driven condensates [32–35], but we are not aware of any theory that explains our results. Incidentally, our large- ϵ data are closer to $n_0 \propto \epsilon^{2/3}$ scaling, and the energy spectrum for the hydrodynamic vortex turbulence is [21] $E(k) \propto \epsilon^{2/3} k^{-5/3}$, but this similarity is likely fortuitous; for our system, numerical GPE simulations [15] show presence of some vortices, but our $E(k) \propto k^{4-\gamma}$ has a different k -dependence.

To further explore the analogy between equilibrium state variables and our n_0 and ϵ , we study the response of a turbulent gas to dynamical changes in the driving force (Fig. 3). In equilibrium, state variables have no memory of the history of the system. Here, we prepare one of the two steady states shown in Fig. 2a (with $U_D/k_B = 150$ nK), then suddenly quench F_0 , either from μ/L to $3\mu/L$ or vice versa, and show that the new steady state indeed has the same ϵ (Fig. 3a) and n_0 (Fig. 3b) as if F_0 had always been equal to its new value.

We also briefly look at the state-switching dynamics, when the system ‘re-equilibrates’ to the new (non-equilibrium) steady state. Following the quench of F_0 , it takes a nonzero time for the flux change at k_F to propagate to k_D [16, 29], just like it takes a nonzero time to initially establish a turbulent steady state starting from equilibrium. In Fig. 3b, blue and purple curves illustrate, for the increased and decreased F_0 respectively, how the change in n_k propagates from low to high k , with the local (in k -space) cascade population increasing for the blue curve and decreasing for the purple one; note that in the latter case some atoms return to low k . During the switching between steady states, n_0 is not defined, so to simply quantify the quench dynamics in Fig. 3c we show how the total cascade populations approach their new steady-state values.

Having established n_0 and ϵ as good state variables, in Fig. 4 we generalise our measurements of $n_0(\epsilon)$ to different interaction strengths and gas densities, *i.e.*, different initial equilibrium states (see Fig. 1a). For two data sets we also vary the box length, and hence $k_F = \pi/L$. In Fig. 4a we show that the relationship between n_0 and ϵ is not unique for different a and n ; here, for the same n_0 the underlying flux varies by more than an order of magnitude.

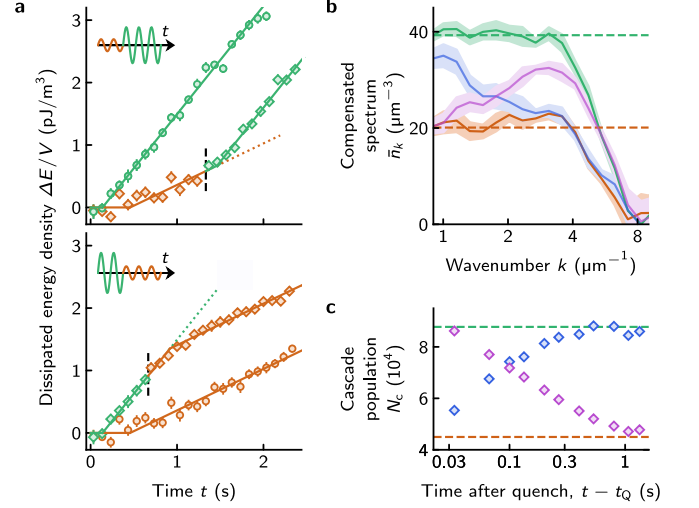


FIG. 3. Switching between turbulent steady states. Quenches of the drive strength show that the steady-state n_0 and ϵ , like equilibrium state variables, do not depend on the history of the system. Here the parameters are the same as in Fig. 2a and we quench F_0 either from μ/L to $3\mu/L$ (‘up quench’) or vice versa (‘down quench’). **a**, The orange and green diamonds, respectively, correspond to the smaller and larger F_0 , the black dashed lines indicate the quench times t_Q , and the circles show reference data taken with constant F_0 . For both up (top panel) and down (bottom panel) quench, the post-quench data is parallel to the reference one, showing that ϵ are the same. The small delays between t_Q and the changes in ϵ measured at k_D reflect the need for the flux change to propagate through k -space. **b**, The green and orange curves, respectively, show the steady-state compensated spectra after the up and down quenches, and the dashed lines show the reference n_0 values from Fig. 2a. We also show examples of transient \bar{n}_k , during the switching between the steady states, for the up (blue, $t - t_Q = 0.03$ s) and down (purple, $t - t_Q = 0.13$ s) quenches. **c**, State-switching dynamics seen in the total number, N_c , of atoms in the cascade (Methods), for the up (blue) and down (purple) quenches; the dashed lines show steady-state values. The shading in **b** and the error bars in **a** and **c** (often smaller than symbol sizes) show standard errors of measurement.

However, we empirically find that all the data can be collapsed onto a universal EoS using simple scaling with a and n (Fig. 4b). Since the experimental EoS is not simply a power-law, even for single (a, n) (Fig. 2c), it can be universal only in a completely dimensionless form, but this requirement does not lead to unique scaling predictions: ϵ can be scaled into dimensionless form by $\hbar^3 n^3 a^2 m^{-2} (na^3)^\delta$ with any δ , and n_0 can be scaled by $n(na^3)^\theta$ with any θ . Using δ and θ as the only free parameters, we find good data collapse for $\delta = 0.13$ and $\theta = 0.19$ (Methods); note that here we do not presume the shape of the universal EoS, treat all the data points in Fig. 4a together as a single data set, and use δ and θ to simply minimise the data scatter. To further verify our results, we extract n_0 and ϵ from an experiment with a ^{87}Rb gas [15] (Methods); this additional data point also agrees with our universal curve.

Even for low (scaled) ϵ these a and n scalings are not explained by the perturbative WWT theory, where the cascade

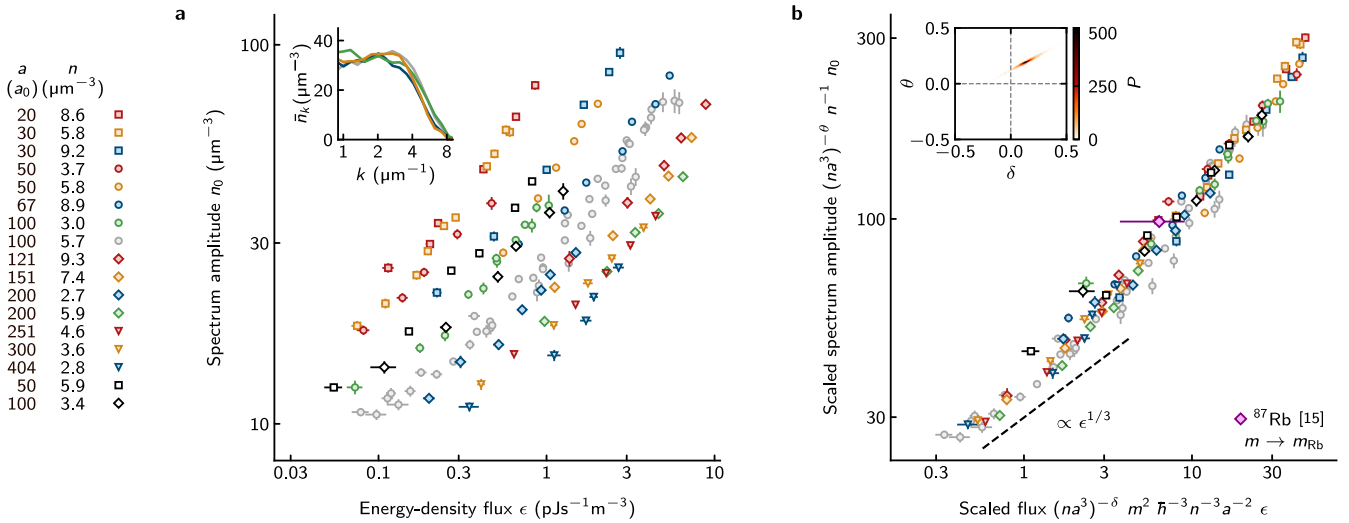


FIG. 4. **Universal equation of state.** We generalise the measurements of $n_0(\epsilon)$ to different interaction strengths a and gas densities n ; all the data from Fig. 2c are here shown in grey. The black symbols indicate data sets for which the injection scale was also changed from $k_F = 0.06 \mu\text{m}^{-1}$ by varying the box length (squares: $k_F = 0.04 \mu\text{m}^{-1}$, diamonds: $k_F = 0.08 \mu\text{m}^{-1}$). **a**, The EoS $n_0(\epsilon)$ is not universal for different a and n . The inset shows four steady-state \bar{n}_k with the same $n_0 \approx 32 \mu\text{m}^{-3}$ but fluxes that vary between 0.28 and $3.4 \text{ pJ s}^{-1} \text{m}^{-3}$. **b**, We empirically collapse all the data onto a universal EoS by making both axes dimensionless and allowing additional scaling with the dimensionless parameter na^3 (see text). In the main panel $\delta = 0.13$ and $\theta = 0.19$, while the inset shows the joint probability distribution P for these scaling exponents (Methods). The single purple point shows data extracted from a ^{87}Rb experiment [15], with the appropriate mass scaling included (m_{Rb} denotes the ^{87}Rb mass). The dashed line is a guide to the eye. The error bars show standard fitting errors.

dynamics depend only on n_0 and not on the total density n ; for a direct comparison of the data with this theory see Extended Data Fig. 1c. The fact that the experimental EoS depends on the total n implies that the presence of the condensate is also relevant for the cascade transport. We also note that, even with the condensate included, no GPE-based model is compatible with our data, because in any such model the interaction strength enters only via the product $n \times a$, and n_0/n can be a function of only ϵ/n and na .

Our experimentally constructed EoS provides both support and new challenges for non-equilibrium theories. The fact that a universal EoS for matter-wave turbulence exists at all provides a paradigmatic example of an equilibrium-like description of far-from-equilibrium matter, but the form of this EoS remains unexplained. Our experiments also demonstrate the possibility to study time-resolved transitions between non-thermal stationary states, which would be interesting to investigate further. In particular, an important question is how the transitions between two flux-carrying steady states relate to the turbulent relaxation and thermalization in isolated quantum systems [36–41]. Another important open problem is whether intermittency [42, 43] plays a role in our turbulent gas. Finally, our results could inspire and be relevant for future experiments with other quantum fluids; it would be interesting to study whether universal equations of state can be constructed for turbulence in systems such as Fermi gases, atomic superfluids with dipolar interactions, or the dissipative exciton-polariton condensates, and whether and how they differ from our EoS.

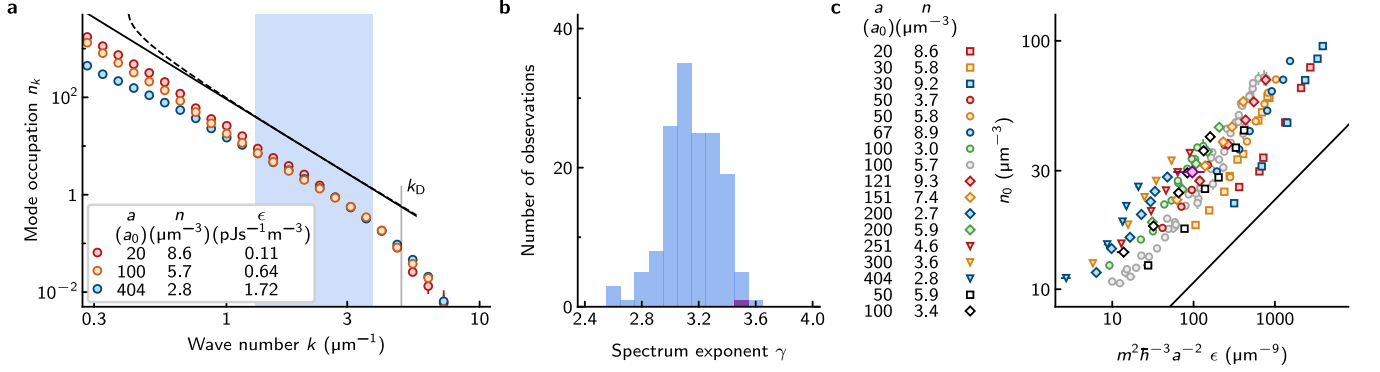
We thank Claudio Castelnovo, Jean Dalibard, Nishant Dogra, Kazuya Fujimoto, Maciej Gałka, Giorgio Krstulovic, Nir Navon, Davide Proment, and Martin Zwierlein for helpful discussions. This work was supported by EPSRC [Grants No. EP/N011759/1 and No. EP/P009565/1], ERC (QBox and UniFlat) and STFC [Grant No. ST/T006056/1]. T. A. H. acknowledges support from the EU Marie Skłodowska-Curie program [Grant No. MSCA-IF- 2018 840081]. A. C. acknowledges support from the NSF Graduate Research Fellowship Program (Grant No. DGE2040434). C. E. acknowledges support from Jesus College (Cambridge). R. P. S acknowledges support from the Royal Society. Z. H. acknowledges support from the Royal Society Wolfson Fellowship.

-
- [1] L. D. Landau and E. M. Lifshitz, *Statistical Physics: Volume 5* (Elsevier Science, 2013).
 - [2] L. F. Cugliandolo, J. Kurchan, and L. Peliti, Energy flow, partial equilibration, and effective temperatures in systems with slow dynamics, *Phys. Rev. E* **55**, 3898 (1997).
 - [3] L. Berthier, G. Biroli, J.-P. Bouchaud, L. Cipelletti, and W. van Saarloos (Eds.), *Dynamical Heterogeneities in Glasses, Colloids and Granular Media* (Oxford University Press, 2011).
 - [4] D. Loi, S. Mossa, and L. F. Cugliandolo, Effective temperature of active matter, *Phys. Rev. E* **77**, 051111 (2008).
 - [5] S. C. Takatori and J. F. Brady, Towards a thermodynamics of active matter, *Phys. Rev. E* **91**, 032117 (2015).
 - [6] F. Ginot, I. Theurkauff, D. Levis, C. Ybert, L. Bocquet, L. Berthier, and C. Cottin-Bizonne, Nonequilibrium Equation

- of State in Suspensions of Active Colloids, *Phys. Rev. X* **5**, 011004 (2015).
- [7] E. Fodor, C. Nardini, M. E. Cates, J. Tailleur, P. Visco, and F. van Wijland, How far from equilibrium is active matter?, *Phys. Rev. Lett.* **117**, 038103 (2016).
- [8] S. F. Edwards and W. D. McComb, Statistical mechanics far from equilibrium, *J. Phys. A: Gen. Phys.* **2**, 157 (1969).
- [9] J. Cardy, G. Falkovich, K. Gawędzki, S. Nazarenko, and O. Zaboronski, *Non-equilibrium Statistical Mechanics and Turbulence*, London Mathematical Society Lecture Note Series (Cambridge University Press, 2008).
- [10] D. P. Ruelle, Hydrodynamic turbulence as a problem in nonequilibrium statistical mechanics, *Proc. Natl. Acad. Sci. U.S.A.* **109**, 20344 (2012).
- [11] A. Picozzi, J. Garnier, T. Hansson, P. Suret, S. Randoux, G. Millot, and D. N. Christodoulides, Optical wave turbulence: Towards a unified nonequilibrium thermodynamic formulation of statistical nonlinear optics, *Phys. Rep.* **542**, 1 (2014).
- [12] N. Navon, R. P. Smith, and Z. Hadzibabic, Quantum gases in optical boxes, *Nat. Phys.* **17**, 1334 (2021).
- [13] V. E. Zakharov, V. S. L'vov, and G. Falkovich, *Kolmogorov spectra of turbulence I: Wave turbulence* (Springer Berlin, 1992).
- [14] S. Nazarenko, *Wave turbulence* (Springer, 2011).
- [15] N. Navon, A. L. Gaunt, R. P. Smith, and Z. Hadzibabic, Emergence of a turbulent cascade in a quantum gas, *Nature* **539**, 72 (2016).
- [16] N. Navon, C. Eigen, J. Zhang, R. Lopes, A. L. Gaunt, K. Fujimoto, M. Tsubota, R. P. Smith, and Z. Hadzibabic, Synthetic dissipation and cascade fluxes in a turbulent quantum gas, *Science* **366**, 382 (2019).
- [17] L. F. Richardson, *Weather prediction by numerical process* (Cambridge University Press, 1922).
- [18] P. A. Hwang, D. W. Wang, E. J. Walsh, W. B. Krabill, and R. N. Swift, Airborne measurements of the wavenumber spectra of ocean surface waves. Part I: Spectral slope and dimensionless spectral coefficient, *J. Phys. Oceanogr.* **30**, 2753 (2000).
- [19] L. Sorriso-Valvo, R. Marino, V. Carbone, A. Noullez, F. Lepreti, P. Veltri, R. Bruno, B. Bavassano, and E. Pietropaolo, Observation of Inertial Energy Cascade in Interplanetary Space Plasma, *Phys. Rev. Lett.* **99**, 115001 (2007).
- [20] S. Ghashghaie, W. Breymann, J. Peinke, P. Talkner, and Y. Dodge, Turbulent cascades in foreign exchange markets, *Nature* **381**, 767 (1996).
- [21] A. N. Kolmogorov, The Local Structure of Turbulence in Incompressible Viscous Fluid for Very Large Reynolds' Numbers, *Dokl. Akad. Nauk. SSSR* **30**, 301 (1941).
- [22] H. L. Grant, R. W. Stewart, and A. Moilliet, Turbulence spectra from a tidal channel, *J. Fluid Mech.* **12**, 241 (1962).
- [23] K. R. Sreenivasan, On the universality of the Kolmogorov constant, *Phys. Fluids* **7**, 2778 (1995).
- [24] A. L. Gaunt, T. F. Schmidutz, I. Gotlibovich, R. P. Smith, and Z. Hadzibabic, Bose-Einstein Condensation of Atoms in a Uniform Potential, *Phys. Rev. Lett.* **110**, 200406 (2013).
- [25] C. Eigen, A. L. Gaunt, A. Suleymanzade, N. Navon, Z. Hadzibabic, and R. P. Smith, Observation of Weak Collapse in a Bose-Einstein Condensate, *Phys. Rev. X* **6**, 041058 (2016).
- [26] I. Chantesana, A. Piñeiro Orioli, and T. Gasenzer, Kinetic theory of nonthermal fixed points in a Bose gas, *Phys. Rev. A* **99**, 043620 (2019).
- [27] Y. Zhu, B. Semisalov, G. Krstulovic, and S. Nazarenko, Direct and Inverse Cascades in Turbulent Bose-Einstein Condensates, *Phys. Rev. Lett.* **130**, 133001 (2023).
- [28] J. Etrych, G. Martirosyan, A. Cao, J. A. P. Glidden, L. H. Dogra, J. M. Hutson, Z. Hadzibabic, and C. Eigen, Pinpointing Feshbach resonances and testing Efimov universalities in ^{39}K , *Phys. Rev. Res.* **5**, 013174 (2023).
- [29] M. Galka, P. Christodoulou, M. Gazo, A. Karailiev, N. Dogra, J. Schmitt, and Z. Hadzibabic, Emergence of Isotropy and Dynamic Scaling in 2D Wave Turbulence in a Homogeneous Bose Gas, *Phys. Rev. Lett.* **129**, 190402 (2022).
- [30] J. Zhang, C. Eigen, W. Zheng, J. A. P. Glidden, T. A. Hilker, S. Garratt, R. Lopes, N. Cooper, Z. Hadzibabic, and N. Navon, Many-Body Decay of the Gapped Lowest Excitation of a Bose-Einstein Condensate, *Phys. Rev. Lett.* **126** (2021).
- [31] Y. Sano, N. Navon, and M. Tsubota, Emergent isotropy of a wave-turbulent cascade in the Gross-Pitaevskii model, *EPL* **140**, 66002 (2022).
- [32] M. C. Tsatsos, P. E. S. Tavares, A. Cidrim, A. R. Fritsch, M. A. Caracanhas, F. E. A. dos Santos, C. F. Barenghi, and V. S. Bagnato, Quantum turbulence in trapped atomic Bose-Einstein condensates, *Phys. Rep.* **622**, 1 (2016).
- [33] M. Tsubota, K. Fujimoto, and S. Yui, Numerical Studies of Quantum Turbulence, *J. Low. Temp. Phys.* **188**, 119–189 (2017).
- [34] H. A. J. Middleton-Spencer, A. D. G. Orozco, L. Galantucci, M. Moreno, N. G. Parker, L. A. Machado, V. S. Bagnato, and C. F. Barenghi, Evidence of Strong Quantum Turbulence in Bose-Einstein Condensates, *arXiv:2204.08544* (2022).
- [35] C. F. Barenghi, H. A. J. Middleton-Spencer, L. Galantucci, and N. G. Parker, Types of quantum turbulence, *arXiv:2302.05221* (2023).
- [36] R. Micha and I. I. Tkachev, Turbulent thermalization, *Phys. Rev. D* **70**, 043538 (2004).
- [37] J. Berges, A. Rothkopf, and J. Schmidt, Nonthermal Fixed Points: Effective Weak Coupling for Strongly Correlated Systems Far from Equilibrium, *Phys. Rev. Lett.* **101**, 041603 (2008).
- [38] M. Prüfer, P. Kunkel, H. Strobel, S. Lannig, D. Linnemann, C.-M. Schmied, J. Berges, T. Gasenzer, and M. K. Oberthaler, Observation of universal dynamics in a spinor Bose gas far from equilibrium, *Nature* **563**, 217 (2018).
- [39] S. Erne, R. Bückner, T. Gasenzer, J. Berges, and J. Schmiedmayer, Universal dynamics in an isolated one-dimensional Bose gas far from equilibrium, *Nature* **563**, 225 (2018).
- [40] J. A. P. Glidden, C. Eigen, L. H. Dogra, T. A. Hilker, R. P. Smith, and Z. Hadzibabic, Bidirectional dynamic scaling in an isolated Bose gas far from equilibrium, *Nat. Phys.* **17**, 457 (2021).
- [41] A. D. García-Orozco, L. Madeira, M. A. Moreno-Armijos, A. R. Fritsch, P. E. S. Tavares, P. C. M. Castilho, A. Cidrim, G. Roati, and V. S. Bagnato, Universal dynamics of a turbulent superfluid Bose gas, *Phys. Rev. A* **106**, 023314 (2022).
- [42] G. K. Batchelor, A. A. Townsend, and H. Jeffreys, The nature of turbulent motion at large wave-numbers, *Proc. R. Soc. Lond. A* **199**, 238 (1949).
- [43] A. C. Newell, S. Nazarenko, and L. Biven, Wave turbulence and intermittency, *Phys. D: Nonlinear Phenom.* **152–153**, 520–550 (2001).

Methods

Steady-state momentum distributions. The fact that the driven gas has reached its (quasi-)steady state is signalled by the onset of dissipation (atom loss; see Fig. 2a), and for con-



EXTENDED DATA FIG. 1. **Steady-state momentum distributions and comparison with the perturbative WWT theory.** **a**, Steady-state n_k for three different combinations of a and n , with fluxes ϵ chosen such that the cascade amplitudes are similar. The blue shading shows the k range where we fit all our data. For the data shown here, $1/\xi = 0.48$ (red), 0.87 (orange) and $1.22 \mu\text{m}^{-1}$ (blue). Fitted with γ as a free parameter, these spectra give $\gamma = 3.3$ (red), 3.0 (orange) and 3.1 (blue). The solid line shows $n_0 k^{-3} (k\xi)^{-0.2}$ and the dashed line shows $n_0 k^{-3} \ln(k/k_0)^{-1/3}$ with the same n_0 (chosen such as to offset the curves from the data for clarity), ξ corresponding to the orange data, and $k_0 = 0.4 \mu\text{m}^{-1}$. The error bars show standard errors of measurement. **b**, Histogram of extracted γ for all spectra corresponding to the 153 points in Fig. 4, when fitting $n_k \propto k^{-\gamma}$ with γ as a free parameter. The purple bar indicates the Rb data point. **c**, Comparison of all the data shown in Fig. 4 with the perturbative WWT theory [27] (solid line), without any free parameters. The error bars show standard fitting errors.

sistency we always measure n_k at the time when the atom number is reduced from its initial value by 15%. We obtain n_k from time-of-flight images, setting $a = 0$ during the expansion, combining measurements for expansion times between 12 and 78 ms (with each measurement repeated 3 - 6 times), and reconstructing the three-dimensional distributions with the inverse Abel transformation [40]. We normalise n_k so that the total atom number is $N = (2\pi)^{-3} V \int n_k 4\pi k^2 dk$.

As illustrated in Extended Data Fig. 1a for different experimental parameters, our n_k are close to power-laws in a k -range $1/\xi \lesssim k \lesssim 0.8 k_D$; the examples shown here span the full range of $1/\xi$ values in Fig. 4. To treat all data equally, we conservatively always fit n_k between $k_{\min} = 1.3 \mu\text{m}^{-1}$ and $k_{\max} = 3.8 \mu\text{m}^{-1}$ (blue shading in Extended Data Fig. 1a), so $k_{\min} > 1/\xi$ is always satisfied. Similarly, the cascade population N_c in Fig. 3 is defined as the atom number at $k > k_{\min}$.

Extended Data Fig. 1b shows the histogram of the fitted γ values for all the spectra corresponding to the 153 data points in Fig. 4; we find a mean $\gamma = 3.2$ with a standard deviation of 0.2. Various analytical and numerical calculations [13, 14, 26, 27] give that in our finite k range one expects an effective $\gamma - 3 \lesssim 0.5$. Specifically, the analytical WWT prediction [13, 27] for $n_0(\epsilon)$ is based on $n_k = n_0 k^{-3} f(k)$ with $f(k) = \ln(k/k_0)^{-1/3}$. In this calculation, particles are injected isotropically at k_0 and the results formally hold for $k \gg k_0$. We inject energy (anisotropically) at a very low k_F , in the phonon regime, but the onset of the isotropic cascade should still be at $k \sim 1/\xi$ [29, 31]. Empirically, varying k_0 between $0.06 \mu\text{m}^{-1}$ (our k_F) and $0.6 \mu\text{m}^{-1}$ (just a factor of two smaller than k_{\min}), the analytical curves are, between k_{\min} and k_{\max} , always fitted well by power laws and give effective γ between 3.1 and 3.3; our mean $\gamma = 3.2$ is reproduced by setting $k_0 = 0.4 \mu\text{m}^{-1}$ (see Extended Data Fig. 1a).

To consistently extract the cascade amplitudes n_0 with di-

mensions of μm^{-3} , we refit all the data with fixed $\gamma = 3.2$ and define n_0 via $n_k = n_0 k^{-3} (k\xi)^{-0.2}$, i.e., we model $f(k)$ by $(k\xi)^{-0.2}$ in our fitting range. We use ξ as the natural scale for making f dimensionless, but using a constant $\bar{\xi} = 1.3 \mu\text{m}$ (the geometric mean of our ξ range) would change the n_0 values by only $\pm 10\%$ and not alter any conclusions. Modelling $f = (Ak\xi)^{-0.2}$ with a constant dimensionless $A \neq 1$ would be equally valid, simply rescaling n_0 by a constant and not affecting the EoS shape, but $A = 1$ is both the simplest choice and makes our heuristic f almost equal (within $\lesssim 10\%$ in our fitting range) to the analytical WWT one with $k_0 = 0.4 \mu\text{m}^{-1}$ (see Extended Data Fig. 1a), which allows a fair comparison of our n_0 with this theory (Extended Data Fig. 1c).

Comparison with the perturbative WWT theory. Extended Data Fig. 1c shows the comparison of all our experimental n_0 values for different a and n (Fig. 4) with the most recent perturbative WWT calculation [27] (dashed line), without any free parameters. The theoretical and experimental n_0 agree within a factor of 3, but the theoretical scaling $n_0 \propto (m^2 \hbar^{-3} a^{-2} \epsilon)^{1/3}$, which does not depend on n , does not collapse the data onto a single curve.

The universal EoS. To find the optimal scaling exponents in Fig. 4, for any given (δ, θ) we quantify the collapse of the scaled data using the reduced χ^2 of a simple piece-wise power-law fit (allowing for four x -axis regions with different power laws) to all the data points, without distinguishing different a and n . For $\delta = \theta = 0$ we get $\chi^2 = 47$, while for the optimal $\delta = 0.13$ and $\theta = 0.19$ we get $\chi^2 = 3.8$. We get essentially the same $\chi^2 = 3.5$ for the single- (a, n) data series shown in Fig. 2c, which suggests that with optimal δ and θ all the dependence on a and n has been scaled out. The fact that these χ^2 are larger than 1 suggests that the data scatter is not purely statistical, but also comes from systematic errors. These could arise, for example, due to the small residual in-

homogeneity of gases trapped in optical boxes [12]. For completeness, note that for the WWT scaling in Extended Data Fig. 1c we get $\chi^2 = 57$.

To construct the joint probability distribution $P(\delta, \theta)$ (inset of Fig. 4b) we randomly select 1/3 of the data, apply the same optimisation procedure, and repeat this 10^4 times. Treating δ and θ as independent variables with Gaussian distributions gives standard deviations $\sigma_\delta = 0.08$ and $\sigma_\theta = 0.04$. However, the errors in the two exponents are correlated, as seen from the shape of $P(\delta, \theta)$, and the peak probability density, $P(0.13, 0.19) \approx 500$, is ten times larger than the Gaussian result $1/(2\pi\sigma_\delta\sigma_\theta) \approx 50$.

Rb data point in Fig. 4. The Rb point further illustrates the universality of the EoS because it is a measurement with an atom of a different mass, performed with a different experimental apparatus. We extracted this data point from Ref. [15]; we obtained n_0 from the spectrum shown in Fig. 3a of that paper (applying the inverse Abel transform and fitting it with $\gamma = 3.2$) and deduced ϵ from the populations shown in the inset of Fig. 3b in that paper. As for our data, for scaling n_0

and ϵ in Fig. 4b we use the initial n .

Data availability The data that support the findings of this study are available in the Apollo repository (<https://doi.org/10.17863/CAM.96408>). Any additional information is available from the corresponding authors upon reasonable request.

Author contributions L. H. D. led the data collection and analysis, with most significant contributions from G. M. and T. A. H. All authors (L. H. D., G. M., T. A. H., J. A. P. G., J. E., A. C., C. E., R. P. S., and Z. H.) contributed significantly to the experimental setup, the interpretation of the results and the production of the manuscript. Z. H. supervised the project.

Competing interests The authors declare no competing interests.

Correspondence and requests for materials should be addressed to L. H. D. (lhb31@cam.ac.uk), C. E. (ce330@cam.ac.uk), or Z. H. (zh10001@cam.ac.uk).

Reprints and permissions information is available at www.nature.com/reprints.